Thermal Modeling and Simulation of a Smart Wrist-worn Wearable Device

Kodai Matsuhashi[1], Koutaro Hachiya[2], Toshiki Kanamoto[1], Masasi Imai[1], and Atsushi Kurokawa[1*]

[1]Graduate School of Science and Technology, Hirosaki University, Aomori, Japan
[2]Graduate Program in Environmental Information Science, Teikyo Heisei University, Tokyo, Japan
[*]kurokawa@eit.hirosaki-u.ac.jp

Abstract – We propose a thermal-circuit model that can calculate temperatures in important places for thermal designs of smart wrist-worn wearable devices. The thermal model can be applied to various wrist-worn wearable devices, which consist of different device-body shapes, belt sizes, and materials. The temperatures obtained using the proposed model agree well with those obtained by a commercial thermal solver. Moreover, by simulations applying the model, we present important knowledge for thermal designs of wrist-worn wearable devices.

I. Introduction

The forecast for worldwide shipments of wearable devices (estimated by Garter) was the 178.91 million in 2018, and it is expected to reach 453.19 million in 2022 [1]. Wrist-worn devices (e.g., smart watches, smart bands, smart bracelets, and fitness trackers) account for over half of the wearable devices in the market, and they are provided by vendors such as Apple, Xiaomi, and Fitbit [2].

Wrist-worn wearable technologies have been researched in domains such as medicine and healthcare, sport, education, human-computer interaction, and security [3, 4]. Wrist-worn wearable devices use many sensors, including accelerometers, gyroscopes, magnetometers, pressure gauges, GPS, thermistors, and piezoelectric devices. Additionally, these devices can measure numerous parameters, such as body movement, physical activity, temperature, and heart rate. The touch interface of smart watches has been presented [5]. Recently, technologies exploiting the temperature difference across a person's body to generate power by so-called "body-heat harvesting" have also been proposed [6, 7].

In regard to current commercial products, battery capacity is small, and battery charging is not easy with current technologies. Furthermore, users expect such devices to have a long operational life in the manner of traditional watches. Under those circumstances, power consumption of most wrist-worn devices (like smart watches) is kept to less than 200 mW [8]. In contrast, power consumption of smart phones ranges from 0.5 to 3 W [9]. Thermal analysis and management of smart phones have been presented [9, 10].

Thermal designs of wrist-worn wearable devices are sparsely reported [11, 12]. To create future smart wrist-worn wearable devices, it will be necessary to process more data at higher speed by using the state-of-the-art sensors and software technologies. In the near future, wrist-worn wearable devices with functions and performance that exceed smart phones may be developed. Technologies for more efficiently charging those devices may also be developed. Further, scenarios in which such devices are used in the manner of high power consumption in a short time may increase. Users of wrist-worn wearable devices might wear the device for different periods of time: all day long (for daily health care such as patient monitoring); half a day or so (for only going out); or short times (such as during sports activities, driving, rehabilitation, and fitness training). Low-temperature burns may be caused if a device with operating temperature of 48°C is in contact with the skin for 10 minutes or if the device with that of 43°C is in contact with the skin for eight hours or longer [11].

In this paper, a new model for thermal designs of smart wrist-worn wearable devices is proposed. Moreover, some important things for thermal designs are presented.

The rest of the paper is organized as follows. Section II describes the smart wrist-worn wearable device used in this work. Section III presents a thermal model for thermal designs of wrist-worn wearable devices. Section IV presents simulation results obtained using the thermal model. Section V concludes this paper.

II. Wrist-worn Wearable Device

A. Overview of Wrist-worn Wearable Device

A model of the wearable device used in this work is shown in Fig. 1. The dimensions of the main parts of the device are shown in Fig. 2, where (a) is a top of view and (b) is a cross section of the wrist when the device is worn around the wrist. Under the basic conditions, device body size is 40×40×11 mm. As a human-body thermal model, a simple model (which assumes that regulatory sweating and skin-blood-flow rate contribute to the core temperature) was used in reference to a two-node model [13].

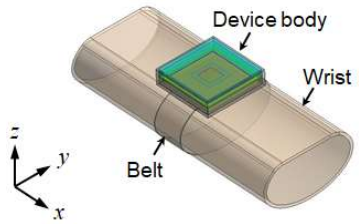

Fig. 1. Overview of wrist-worn wearable device used in this work.

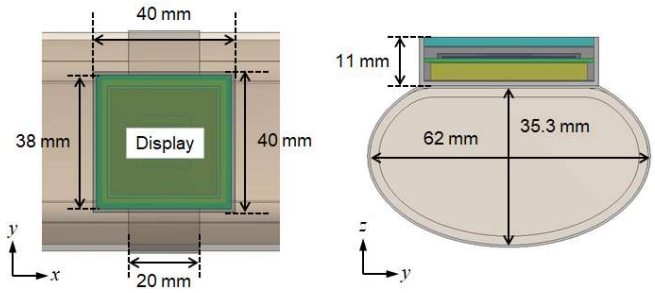

(a) Top view (b) Cross section

Fig. 2. Dimensions of basic structure of the device.

B. Structure and Materials of Wrist-worn Wearable Device

The body of the wrist-worn wearable device, which is composed of a display, 3D IC, package, PCB, battery, and case, is illustrated in Fig. 3(a), and the package containing the 3D IC on the PCB is shown in Fig. 3(b). Size and thermal conductivity of the main parts are listed in Table I. Aluminum was used for the case and belt.

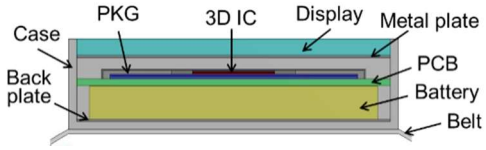

(a) Device body

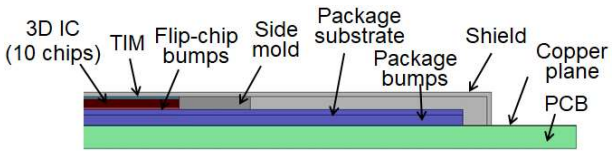

(b) Package with IC

Fig. 3. Structures of main parts of wrist-worn wearable device.

TABLE I
Thermal Conductivity and Size in Basic Conditions of Main Parts

Parts	TC (W/mK)	Size (mm)
Display	x=1.8, y=1.8, z=0.1	x=38, y=38, z=2
Metal plate	10	x=38, y=38, z=0.3
Battery	x=15, y=15, z=10	x=35, y=35, z=4
Back plate	10	x=38, y=38, z=0.25
Case (Al)	236	x=40, y=40, z=11
Belt (Al)	236	l=167, w=20, t=0.5

III. Thermal Modeling

A method for modeling the thermal circuits of wrist-worn wearable devices is proposed on this section.

A. Thermal Circuit Model of 3D IC

An electronic device is generally composed of multiple packages with several chips that include a CPU and memories on a PCB. For simplicity, it is assumed that the 3D IC depicted in Fig. 4 is used for the electronic device. One chip is composed of a metal layer, a device layer, and a chip substrate with through-silicon vias (TSVs). Micro-bumps are used for connecting the chips. Each layer of the 3D IC structure is modelled as an equivalent thermal resistance to be connected in series in the vertical direction.

A simple thermal-circuit model for a 3D IC with multiple heat sources is illustrated in Fig. 5. This model reduces a thermal circuit shown in the form of a one-dimensional-heat-flow model for an n-chip stacked 3D IC (on the left of the figure) to a simple model (on the right of the figure). Thermal resistances of the chip substrate, device layer, metal layer, and micro-bumps are represented by R_{CS}, R_{DL}, R_{ML}, and R_{MB}, respectively. The simple model is reduced to two heat sources (P_{C_U} and P_{C_L}) and three thermal resistances (R_T, R_U, and R_L). The power consumptions for upper and lower chips is represented by

$$P_{C\_U} = \frac{1}{\sum_{i=1}^{n-1} R_i} \times \sum_{i=1}^{n-1} \left(\left(\sum_{j=i}^{n-1} R_j \right) P_{C,\,i} \right), \tag{1}$$

$$P_{C\_L} = \sum_{i=1}^{n} P_{C,\,i} - P_{C\_U}, \tag{2}$$

where $P_{C,i}$ is the power consumption of the i-th chip and R_k $(k = 1, \cdots, n-1)$ is expressed by

$$R_k = R_{DL\_z,\,k} + R_{CS\_z,\,k} + R_{MB\_z,\,k+1} + R_{ML\_z,\,k+1} + R_{DL\_z,\,k+1}. \tag{3}$$

In the simple model shown in Fig. 5, R_T is total thermal resistance between two heat sources, which is calculated as

$$R_T = \sum_{i=1}^{n} R_i, \tag{4}$$

and upper and lower resistances R_U and R_L are expressed as

$$R_U = R_{CS\_z,\,n} + R_{DL\_z,\,n}, \tag{5}$$

$$R_L = R_{DL\_z,\,1} + R_{ML\_z,\,1}. \tag{6}$$

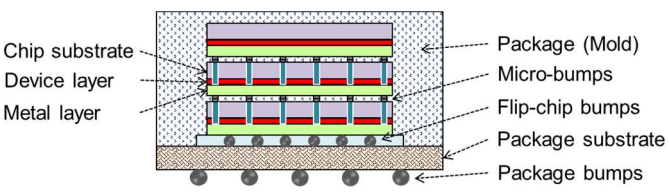

Fig. 4. Illustration of 3D IC structure.

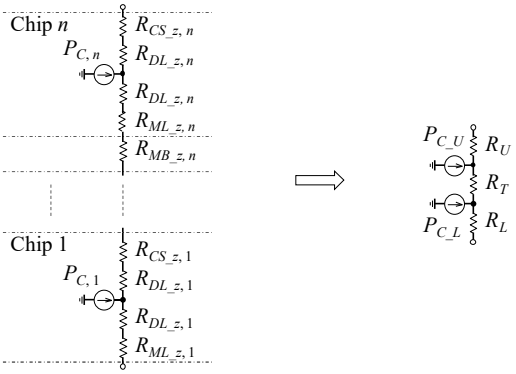

Fig. 5. Simple thermal circuit model for 3D IC with multiple heat sources.

B. Thermal Circuit Model of Case Part

A thermal-circuit model of the case of the device is shown in Fig. 6. The case is a box shape without a cover. Each side is modeled by a series connection of two equivalent thermal resistances in the vertical direction (z direction). The intermediate node is connected with two thermal resistances in the horizontal direction (x and y directions). One resistance (R_{Case_h2}), representing outside the case, is connected with the resistance of ambient air ($R_{Case\_h\_A}$). Natural convection is used as the boundary condition of heat dissipation to the air.

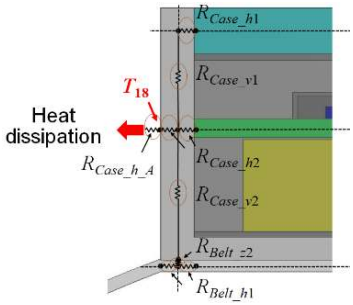

Fig. 6. Thermal circuit model of case part.

C. Thermal Circuit Model of Display

A thermal-circuit model of the display of the device is shown in Fig. 7. The display is modeled by six thermal resistances (R_{Disp_xy} ×4 and R_{Disp_z} ×2) for the ±x, ±y, and ±z directions from a node in the center of the cuboid display. R_{Disp_A} represents thermal resistance of the heat-transfer path from the surface of the display to the atmosphere. Temperature of the display surface is given as T_{17} at the node between R_{Disp_A} and R_{Disp_z}. The metal plate and air between the display and the IC package are modeled as series resistances in the vertical direction only.

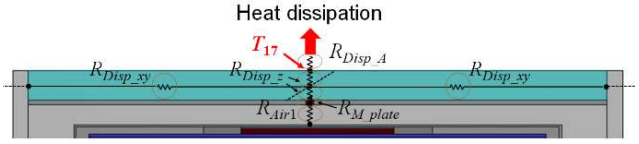

Fig. 7. Thermal circuit model of display.

D. Thermal Circuit Model of Battery

The thermal-circuit model of the battery is shown in Fig. 8. The battery is modeled by only one thermal resistance in the vertical direction (z direction). The top and bottom regions of the battery are also each modelled by a thermal resistance in the vertical direction only. The materials under the battery are also modeled by resistances. T_{13} indicates the temperature at the node between the belt and skin.

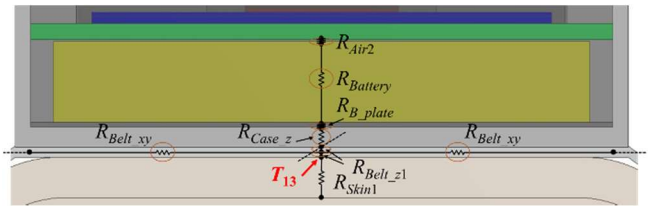

Fig. 8. Thermal circuit model of battery.

E. Thermal Circuit Model of Belt

The thermal-circuit model of the belt and wrist when the device is worn on the wrist is shown in Fig. 9. The length direction of the belt is modeled by six thermal resistances connected in series. To connect the belt and wrist with the ambient air, the outside of the belt is modeled by three thermal resistances. Similarly, to connect them with the rest of the wearer's body, the inside of the belt is modeled by three thermal resistances. Heat-transfer paths from the belt to the atmosphere are represented by $R_{Belt\_h\_A}$ ×2 and $R_{Belt\_v\_A}$ ×1.

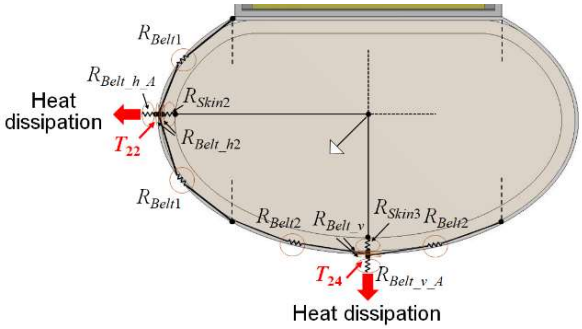

Fig. 9. Thermal circuit model of belt.

F. Whole Model

The whole thermal-circuit model for the wrist-worn wearable device, which combines the models described in Subsections *B* to *E*, is shown in Fig. 10. The total number of thermal-resistance elements is only 83. In the figure, P_D represents power consumption (heat source) of the display.

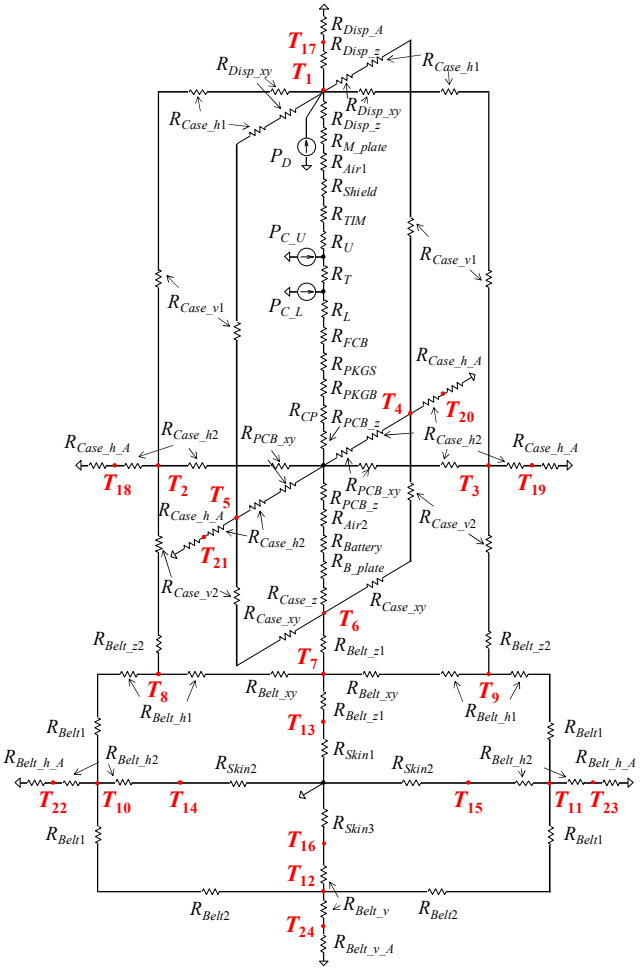

Fig. 10. Entire model for wrist-worn wearable device.

G. Verification of Whole Model

The proposed thermal model is verified as follows. The temperature obtained by using the model in Fig. 10 and that obtained by using the commercial thermal solver [15] are compared in Fig. 11. In the figure, "node number" corresponds to the subscript number of the temperatures in Fig. 10. The results (temperatures) given by the model agree well with the results given by the solver. Maximum error in temperature rise to ambient temperature of 27°C was 4.5%.

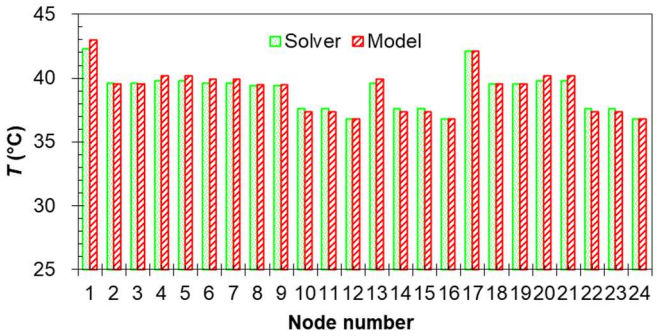

Fig. 11. Comparison of temperatures obtained by the model and solver.

IV. Thermal Simulation

The whole thermal model was applied under various conditions (such as device body shape and belt size) to thermally simulate the device. The basic conditions of the simulation are given as follows. Size of the rectangular device body was 40×40×11 mm. Power consumption of the display was 0.3 W, and total power consumption (including that of the 3D IC) was 1.5 W. Width, length, and thickness of the belt were 20, 167, and 0.5 mm, respectively, and the belt is made of aluminum. Core temperature was 36.6°C, and ambient temperature was 27°C.

Positions of temperatures obtained by the thermal simulations are indicated in Fig. 12. In simulation results, "display" indicates the position at the center of the top surface of the display, "device" indicates the position on the back side of the belt under the device body, and "belt" indicates the position on the back side of the belt, in the middle of the belt.

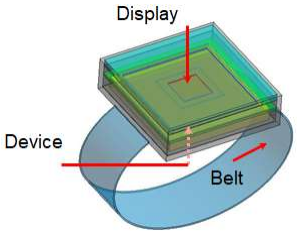

Fig. 12. Positions of temperatures obtained by thermal simulations.

A. Shapes of Device Body

Effects of the shape of the device body on temperature at the top and bottom of the device body were investigated. As for the shape of the device body, a rectangular parallelepiped and an elliptic cylinder are shown in Figs. 13(a) and (b), respectively.

Temperatures at each position in the case of the two different device-body shapes are plotted in Fig. 14, where Figs. 14(a) to (d) respectively show the results obtained by

sizing in the x direction of the rectangular parallelepiped, in the z direction of the rectangular parallelepiped, in the x direction of the elliptic cylinder, and in the z direction of the elliptic cylinder. As the area of the device body (x-sizing) increases, temperature decreases. Similarly, as height of the device body increases (z-sizing), temperature decreases. The area effect is greater than the height effect. The difference in temperature of the rectangular parallelepiped and elliptic cylinder is due to the difference in body areas. Therefore, if the rectangular parallelepiped and elliptic cylinder are the same size in the x- and y-directions, the rectangular parallelepiped is superior from the viewpoint of its temperature-reduction effect.

(a) Rectangular parallelepiped (b) Elliptic cylinder

Fig. 13. Illustration of shapes of device body.

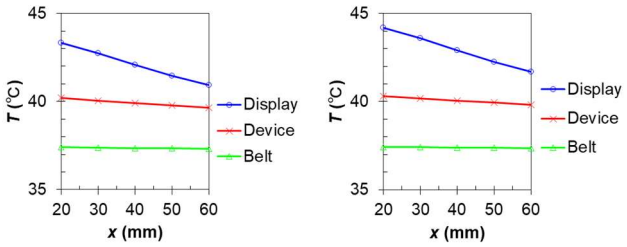

(a) Rectangular shape (b) Elliptical shape

Fig. 14. Effect of device-body shapes on temperature at each part.

B. Effects of Belt Size and Materials on Reduction of Temperature

Belt sizing in terms of width, thickness, and length is illustrated in Fig. 15. Aluminum (thermal conductivity of 236 W/(mK)) was used for the belt material.

The effect of belt radiation obtained by simulations is shown in Fig. 16. Effect of belt width is shown in Fig. 16(a). As the belt width increases, the heat-radiation effect becomes stronger. The belt-width effect is significant because the heat-dissipation area expands. The effect of belt thickness is shown in Fig. 16(b). As belt thickness increases, temperatures at the simulation position of the display and device decrease. However, the effect is saturated at around thickness of 2 mm. Fig. 16(c) shows the effect of belt length. As belt length increases, temperature decreases. However, in the range of practical lengths, the effect is very small. The effect of thermal conductivity of the belt material is shown in Fig. 16(d). While thermal conductivity increases to 50 W/(mK), temperatures at the simulation positions of the display and device decrease significantly. However, when thermal conductivity exceeds about 100 W/(mK), temperature becomes nearly constant.

Difference in temperatures due to belt material (rubber or aluminum) when power consumption was varied is shown in Fig. 17. It is clear that the aluminum belt (which has higher thermal conductivity) is superior in terms of its heat-radiation effect.

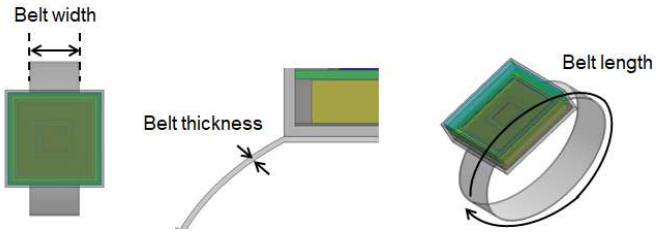

(a) Width (b) Thickness (c) Length

Fig. 15. Illustration of belt sizing.

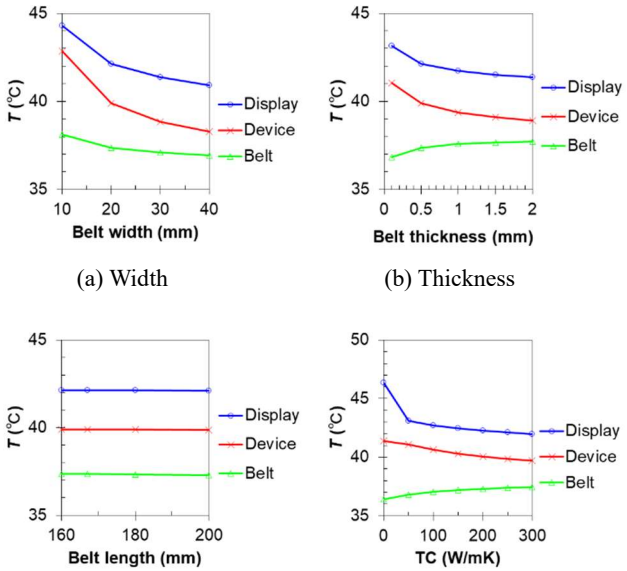

(a) Width (b) Thickness

(c) Length (d) Thermal conductivity

Fig. 16. Effect of belt radiation obtained by varying width, thickness, length, and thermal conductivity.

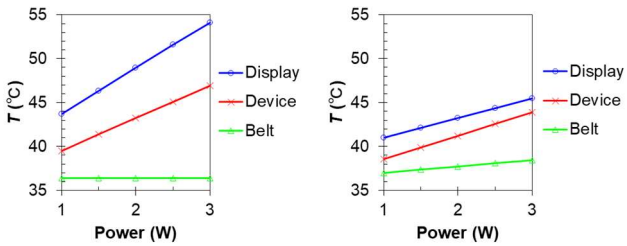

(a) Rubber (b) Al

Fig. 17. Effect on temperature at each part due to belt material.

C. Wrist-worn Belt Effects

The effect of body temperature of the wrist was also examined. In a two-node model, core temperature and skin thickness of the wrist were set to 36.6℃ and 2 mm, respectively.

The effect of the wrist of a person's body on temperature of the wearable device is shown in Fig. 18. It can be seen that the difference in temperature changes when the device is worn on the wrist or not. The temperatures of each part in the case without the wrist, shown in Fig. 18(a), depend on the ambient temperature. The temperatures in the case without the wrist are also important because there is a risk of burns when the device is touched.

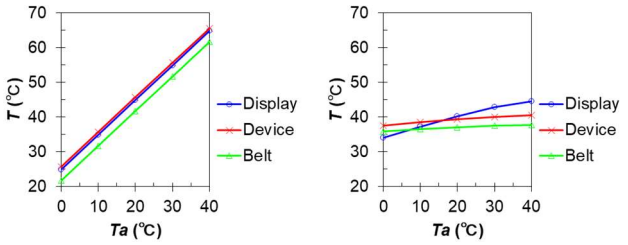

(a) Without wrist (b) With wrist

Fig. 18. Effect of the presence of the wrist on temperature.

V. Conclusion

A thermal model of a smart wrist-worm wearable device was proposed. Although the model is very simple, its accuracy agrees well with that of a commercial thermal solver. In addition, it was shown that the device body with a rectangular shape is superior in terms of temperature-reduction effect to that of the elliptic cylinder, and that the heat-radiation effect of the belt becomes significant if a wide belt made of a material with high thermal conductivity was used.

Acknowledgement

This work was supported by JSPS KAKENHI Grant Number JP17K00070.

References

[1] Garter Inc., "Gartner Says Worldwide Wearable Device Sales to Grow 26 Percent in 2019", https://www.gartner.com/, Nov. 2018.

[2] B2B Newz, "Global Wrist Wearable Market Trend 2019", http://b2bnewz.com/, Apr. 2019.

[3] A. Kamišalić, I. Fister, M. Turkanović, and S. Karakatič, "Sensors and functionalities of non-invasive wrist-wearable devices: A review," *Sensors*, vol. 18, no. 6, pp. 1–33, May 2018.

[4] R. M. Al-Eidan, H. Al-Khalifa, and A. M. Al-Salman, "A review of wrist-worn wearable: sensors, models, and challenges," *J. Sensors*, 5853917, pp. 1–20, Dec. 2018.

[5] S. C. Lim, J. Shin, S. C. Kim, and J. Park, "Expansion of smartwatch touch interface from touchscreen to around device interface using infrared line image sensors," *Sensors*, vol. 15, no. 7, pp. 16642–16653, Jul. 2015.

[6] Y. Shi, Y. Wang, D. Mei, and Z. Chen, "Wearable thermoelectric generator with copper foam as the heat sink for body heat harvesting," *IEEE Access*, vol. 6, pp. 43602–43611, Aug. 2018.

[7] V. Leonov, "Human machine and thermoelectric energy scavenging for wearable devices," *Energy*, vol. 2011, article ID 785380, pp. 1–11, 2011.

[8] X. Liu, T. Chen, F. Qian, Z. Guo, F. X. Lin, X. Wang, and K. Chen, "Characterizing smartwatch usage in the wild," in *Proc. MobiSys*, Jun. 2017, pp. 385–398.

[9] X. Chen, N. Ding, A. Jindal, Y. C. Hu, M. Gupta, and R. Vannithamby, "Smartphone energy drain in the wild: Analysis and implications," in *Proc. SIGMETRICS*, 2015, pp. 151–164.

[10] J. Lee, D. W. Gerlach, and Y. K. Joshi, "Parametric thermal modeling of heat transfer in handheld electronic devices," in *Proc. IEEE ITHERM*, 2008, pp. 604–609.

[11] A. Q. Han, "Thermal management and safety regulation of smart watches," in *Proc. ITherm*, 2016, pp. 939–944.

[12] K. Matsuhashi and A. Kurokawa, "Thermal management for future wrist wearable devices," in *Proc. ICICM*, pp.313-317, Nov. 2018.

[13] A. P. Gagge, J. A. J. Stolwijk, and Y. Nishi, "An effective temperature scale based on a simple model of human physiological regulatory response," *ASHRAE Trans.*, vol. 77, no. 2192, pp. 247–262, 1971.

[14] Femtet® 2018.0.4, Murata Software Co., Ltd., [Online]. Available: http://www.muratasoftware.com/en